Recombinant neutralizing secretory IgA antibodies for preventing mucosal carriage and transmission of SARS-CoV-2

Kathrin Göritzer (kgoritze@sgul.ac.uk)

Hotung Molecular Immunology Unit, 2Institute for Infection and Immunity, St. George's University of London, United Kingdom https://orcid.org/0000-0003-3742-028X

Elisabetta Groppelli

St. George's University of London

Clemens Grünwald-Gruber

Core Facility Mass Spectrometry, University of Natural Resources and Life Sciences, Vienna, Austria

Rudolf Figl

Core Facility Mass Spectrometry, University of Natural Resources and Life Sciences, Vienna, Austria

Fengfeng Ni

State Key Laboratory of Virology, Wuhan Institute of Virology, Center for Biosafety Mega-Science, Chinese Academy of Sciences, Wuhan, China

Huimin Hu

State Key Laboratory of Virology, Wuhan Institute of Virology, Center for Biosafety Mega-Science, Chinese Academy of Sciences, Wuhan, China

Yuncheng Li

State Key Laboratory of Virology, Wuhan Institute of Virology, Center for Biosafety Mega-Science, Chinese Academy of Sciences, Wuhan, China

Yalan Liu

State Key Laboratory of Virology, Wuhan Institute of Virology, Center for Biosafety Mega-Science, Chinese Academy of Sciences, Wuhan, China

Qinxue Hu

State Key Laboratory of Virology, Wuhan Institute of Virology, Center for Biosafety Mega-Science, Chinese Academy of Sciences, Wuhan, China

Rama Devudu Puligedda

Lankenau Institute for Medical Research, Wynnewood, PA, United States

Richard Strasser

Department of Applied Genetics and Cell Biology, University of Natural Resources and Life Sciences, Vienna, Austria

Scott Dessain

Lankenau Institute for Medical Research, Wynnewood, PA, United States

Julian Ma
Hotung Molecular Immunology Unit, Institute for Infection and Immunity, St. George's University of London, United Kingdom https://orcid.org/0000-0003-0767-0042

Article

Keywords: SARS-CoV-2, monoclonal antibodies, virus neutralization, mucosal antibodies, secretory IgA, passive immunisation, plantibodies, molecular pharming

Posted Date: November 29th, 2021

DOI: https://doi.org/10.21203/rs.3.rs-1053315/v1

Recombinant neutralizing secretory IgA antibodies for preventing mucosal carriage and transmission of SARS-CoV-2

Kathrin Göritzer[1*], Elisabetta Groppelli[2], Clemens Grünwald-Gruber[3], Rudolf Figl[3], Fengfeng Ni[4], Huimin Hu[4], Yuncheng Li[4], Yalan Liu[4], Qinxue Hu[2,4], Rama Devudu Puligedda[5], Richard Strasser[6], Scott Dessain[5] and Julian Ma[1].

[1]Hotung Molecular Immunology Unit, [2]Institute for Infection and Immunity, St. George's University of London, United Kingdom

[3]Core Facility Mass Spectrometry, University of Natural Resources and Life Sciences, Vienna, Austria

[4]State Key Laboratory of Virology, Wuhan Institute of Virology, Center for Biosafety Mega-Science, Chinese Academy of Sciences, Wuhan, China

[5]Lankenau Institute for Medical Research, Wynnewood, PA, United States

[6]Department of Applied Genetics and Cell Biology, University of Natural Resources and Life Sciences, Vienna, Austria

***Correspondence:**

Corresponding Author

kgoritze@sgul.ac.uk

Keywords: SARS-CoV-2, monoclonal antibodies, virus neutralization, mucosal antibodies, secretory IgA, passive immunisation, plantibodies, molecular pharming;

Summary

Passive delivery of antibodies to mucosal sites might be a valuable adjunct to COVID-19 vaccination to prevent infection, treat viral carriage, or block transmission. However, monoclonal IgG antibody therapies, currently used for treatment of severe infections, are unlikely to prove useful in mucosal sites where SARS-CoV-2 resides and replicates in early infection. Here, we investigated the feasibility of producing neutralising monoclonal IgA antibodies against SARS-COV-2. We identified two class-switched mAbs that express well as monomeric and secretory IgA variants with retained antigen binding affinities and increased stability in mucosal secretions compared to their IgG counterparts. SIgAs had stronger virus neutralisation activities than IgG mAbs and were able to reduce SARS-CoV-2 infection in an *in vivo* murine model. Our findings provide a persuasive case for developing recombinant SIgAs for mucosal application as a new tool in the fight against COVID-19.

Introduction

COVID-19 is a mucosal infection caused by SARS-CoV-2. The virus replicates in the respiratory tract and is transmitted through respiratory droplets produced when an infected person coughs, sneezes, or talks. The most prominent symptoms of COVID-19 affect the respiratory system (continuous cough, shortness of breath), but in some cases sensory tissues in the upper respiratory tract are involved causing anosmia and loss of taste [1]. Additionally, gastro-intestinal symptoms (nausea, vomiting and diarrhea) are reported in 6% of adults and up to 20% in children [2]. Virus can be detected at all these sites as well as in urine [3].

Infection with SARS-CoV-2 elicits systemic and mucosal immune responses [4]. Whilst attention has been focused on serum antibody responses which are dominated by IgG, at mucosal sites such as the respiratory, gastrointestinal, and genitourinary tracts, immunoglobulin A (IgA) in the external secretions that bathe mucosal surfaces is the predominant antibody class [5]. Mucosal IgA in SARS-CoV-2 can be neutralising and long-lasting [4].

Various co-morbidities have been associated with diminished immune responses to SARS-CoV-2, including immunosuppressive drugs to prevent transplant failure and diabetes [6]. Seroconversion following COVID-19 vaccination can also be compromised in these and similar patients [7, 8]. In such circumstances, passive delivery of antibodies might be a valuable adjunct to COVID-19 vaccination, in which neutralising antibodies could be delivered directly to mucosal sites either to prevent infection, treat viral carriage or block transmission. Furthermore, topical delivery of antibodies could be useful to prevent carriage of virus in asymptomatic individuals.

Neutralising monoclonal IgG antibodies [9] are already approved for systemic use in early SARS-CoV-2 treatment, but are unlikely to prove useful in mucosal fluids which are non-sterile and rich in endogenous and exogenous proteases [10]. For mucosal sites, IgA in the form of secretory

IgA (SIgA), would be preferred, as the polymeric complex is adapted for the harsh, unstable external mucosal environment [11]. The potential for this approach has previously been demonstrated in other model mucosal infections [12, 13, 14].

However, monoclonal SIgA antibodies are technically challenging to produce. The first recombinant approach to expressing secretory antibodies was in genetically modified plants [15]. Other approaches have been described [16, 17, 18], but still seem impractical or unaffordable for commercial development. Some improvements to SIgA expression have been reported in plants [19, 20, 21, 22] which still seems the most promising approach.

In this study, we investigated the feasibility of producing neutralising monoclonal IgA antibodies against SARS-CoV-2. Starting with IgG class mAbs, we expressed monomeric and secretory forms of IgA and compared these for their functionality and stability. Finally, we assessed the potential use of SIgA to prevent SARS-CoV-2 infection in an *in vivo* model.

Experimental procedures

Construct design and cloning

The plant codon-optimized sequences of the heavy and light chain variable regions of COVA2-15 (QKQ15273.1, QKQ15189.1), COVA1-22 (QKQ15169.1, QKQ15253.1), 2-15 (PDB: 7L57_H, 7L57_L) and 2E8 (manuscript submitted) IgG mAbs flanked with BsaI type II restriction sites were synthesized by GeneArt (Thermo Fisher Scientific, USA)[23, 24]. Using Golden Gate assembly, the variable heavy chain sequences were cloned into pDONR based plasmids between a human Ig heavy chain leader sequence ('MELGLSWIFLLAILKGVQC') and either human gamma-1 (AAA02914.1), alpha-1 (AAT74070.1) or alpha-2m(1) (AAT74071.1) constant regions. Variable light chain fragments were inserted between the human light chain leader sequence ('MDMRVPAQLLGLLLLWLPGARC') and either human kappa constant regions for COVA2-15 variants (AAA58989.1) or lambda constants regions for COVA1-22, 2-15 and 2E8 variants (CAA40940.1)[25]. Full length heavy and light chain genes were separately subcloned into the binary high expression vector pEAQ-HT-DEST3 using Gateway cloning [26]. Human secretory component (SC) and joining chain (JC) constructs cloned separately into pEAQ-HT have been described previously [14]. The pEAQ-HT plant expression vectors containing the gamma and alpha heavy chains as well as the kappa and lambda light chains were transformed into *Agrobacterium tumefaciens* strain GV3101 (Leibniz Institut DSMZ-Deutsche Sammlung von Mikroorganismen und Zellkulturen GmbH, DSM 12364) by electroporation.

The construct for expression of the receptor binding domain (RBD) of the SARS-COV-2 spike (PDB-id: 6VYB, R319-F541) with a C-terminal 6xHis-tag cloned into pCAGGS mammalian expression vector was provided by Mark Dürkop from BOKU, Vienna.

Transient expression of IgG and IgA variants in N.benthamiana

Agrobacteria containing the appropriate constructs were grown overnight at 28°C in Lysogeny-Broth (LB) containing 25 µg/mL rifampicin and 50 µg/mL kanamycin. For expression of IgG or monomeric IgA1 and IgA2 variants, the overnight cultures containing the respective constructs for the heavy and light chain were diluted in infiltration buffer (10 mM MES, 10 mM $MgSO_4$, and 0.1 mM acetosyringone) to an OD_{600} of 0.1. For secretory IgA variants, heavy and light chain constructs were diluted to an OD_{600} of 0.05 and mixed with the Joining chain construct at an OD_{600} of 0.2 and the secretory component construct at an OD_{600} of 0.1. *Agrobacteria* solutions were then introduced into 6- to 8-week-old glycoengineered *Nicotiana benthamiana* ΔXT/FT plants by vacuum infiltration [27, 28]. Plants were grown in a controlled environment room at 25°C with an 16/8-hour light/dark cycle. After 5 days, infiltrated leaf material was harvested, and crude leaf extract was prepared by adding 3 volumes of ice-cold phosphate-buffer saline (PBS) pH 7.4 containing 0.1% (v/v) Tween in a blender. Homogenized leaf material was passed through a Miracloth filter (Merck Millipore, Germany) and centrifuged at 20 000 x g for 1h, followed by filtration through 0.45 µm pore size filters (Durapore membrane filter, Merck Millipore, Germany).

Purification of IgG and IgA variants from crude leaf extract

Clarified leaf extracts were subjected to columns packed with either Pierce™ Protein A resin for purification of IgG and COVA2-15 IgA variants or CaptureSelect™ IgA affinity matrix (both Thermo Fisher, US) for purification of 2E8 IgA variants equilibrated with PBS. Proteins were eluted with 0.1 M glycine pH 2.7, followed by immediate addition of 10% (v/v) 1M Tris-HCl pH 9.0 to neutralize the acidic pH. Fractions containing the protein of interest were pooled and dialyzed against PBS at 4°C overnight using a dialyzing cassette with 10 kDa molecular-weight cut off (Slide-A-Lyzer, Thermo Scientific, US). Pooled and dialyzed protein fractions were concentrated using Amicon centrifugal filters with a MWCO of 100 kDa (Merck Millipore, Germany) and subjected to size-exclusion chromatography (SEC) on a HiLoad

16/600 Superdex 200 pg column (GE Healthcare, USA) equilibrated with PBS pH 7.4 connected to an ÄKTA pure (GE Healthcare, USA) FPLC system.

Expression and purification of RBDHis

For production of the recombinant receptor binding domain of the SARS-CoV-2 spike protein, Expi293F™ cells were maintained and transfected according to the manufacturer's manual in FreeStyle™ expression medium (all Thermo Fisher, US). High-quality plasmid preparations were obtained using a Plasmid Midi kit (QUIAGEN, US). For the transfection of 200 mL culture with a cell density of $3.0x10^6$ cells/ml, a total of 200 µg plasmid DNA were mixed in 4 mL OptiPro™ SFM medium and combined with another 4 mL OptiPro™ containing 640 µL ExpiFectamin (all Thermo Fisher, US). The mixture was incubated for 15 minutes before gradual introduction to the cells. The culture was incubated for 7 days at 37°C in a humidified atmosphere with 8% CO_2 on an orbital shaker rotating at 125 rpm. The supernatant containing the secreted soluble protein was harvested by centrifugation at 20 000 x g for 30 minutes at 4°C and additionally filtrated through a 0.45 um Durapore membrane filter (Merx Millipore, Germany). Clarified cell supernatant was diluted 1:2 in loading buffer (20 mM Tris, 500 mM NaCl and 10 mM imidazole). The solution was loaded onto a 5 mL HisTrap HP column (GE Healthcare, US) equilibrated with 5 column volumes of loading buffer, and bound protein was eluted by applying buffer containing 20 mM Tris, 500 mM NaCl and 300 mM imidazole. Fractions containing the protein of interest were pooled and dialyzed against PBS at 4°C overnight using a dialyzing cassette with 10 kDa molecular-weight cut off (Slide-A-Lyzer, Thermo Scientific, United States). Pooled and dialyzed protein fractions were concentrated using Amicon centrifugal filters with a MWCO of 100 kDa (Merck Millipore, Germany).

SDS-PAGE

5 µg of purified mAbs were resolved on a NuPage 4–12% Bis/Tris gel (Life Technologies, UK) and stained with InstantBlue (Expedeon, UK).

ELISA

For quantification of IgG and IgA mAbs in clarified crude extract of infiltrated *N. benthamiana* plants ELISA plates were coated with 250 ng/well anti-human gamma chain antiserum (AU004, Binding Site, UK) and goat pAb to human anti-alpha chain (ab97211, Abcam, UK) in PBS pH 7.4 at 4°C overnight, respectively. After blocking with PBS containing 2% (w/v) BSA and 0.1% Tween 20 (v/v) clarified crude plant extracts were added to the wells in normalized concentrations and incubated for 1.5 h at 37°C. As standards, IgG1/kappa or IgG1/lambda isolated from human myeloma plasma (15154, I5029, Sigma, US), purified human IgA (P80-102, Bethyl, US) and IgA from human colostrum (I2363, Sigma, US) were used. Detection of secretory IgA variants was with mouse anti-secretory component (IgA) antibody (SAB4200787, Sigma, US), followed by HRP-labeled anti-mouse antibody (SAB5300168, Sigma, US). For IgG and monomeric IgA variants, HRP-labeled anti-kappa (A18853, Invitrogen, US) or lambda light chain (ab200966, Abcam, UK) antisera were used. After incubation for 1h at 37°C plates were developed using TMB (Thermo Fisher, US) substrate, the reaction was stopped with 2 M H_2SO_4 and read-out was an Infinite F200 Pro plate reader (Tecan, CH) at 450 nm wavelength.

For determination of the ratio of functional and fully assembled SIgA to total IgA in each size-exclusion fraction, similar ELISA assays were performed. Capture was with 150 ng/well purified recombinant RBDHis or anti-alpha HC antibody (ab97211, Abcam, UK). Purified mAbs were diluted to 2 µg/mL in blocking solution and added to RBD and anti-IgA coated plates in normalized concentrations, and incubated for 1.5 h at 37°C. Detection of secretory component or antibody kappa or lambda chains was as described above.

To determine the binding of the purified recombinant mAbs to SARS-CoV-2 RBD the ELISA plates were coated with 150 ng/well purified recombinant RBD-His and purified mAbs were added to the wells in normalized concentration as above. For detection, HRP-labeled anti-human kappa or lambda light chain antibody were used as above. Half-maximal concentration (EC_{50}) was calculated in GraphPad Prism 9.0.

Competitive ELISA

To determine the capability of purified mAbs to inhibit binding of RBD-His to the Ace2 receptor a competitive binding ELISA was performed. Purified Ace2-Fc was kindly provided by Elisabeth Lobner (BOKU Vienna) and 500 ng/well were coated on an ELISA plate at 4°C overnight, followed by blocking with PBS containing 2% (w/v) BSA and 0.1% Tween 20 (v/v). RBD-His was incubated with varying molar ratios of the different mAbs starting with 2:1 [mAbs:RBD-His] reducing to 0.007:1 for 1h at 37°C before addition to the wells. Binding of RBDHis to Ace2-Fc was detected using an HRP-labeled anti-His antibody (71840, Sigma, US) and plates were developed as described above.

Surface plasmon resonance (SPR) spectroscopy

The binding kinetics of plant-produced IgG and IgA mAbs to SARS-CoV-2 RBD-His were determined on a BIAcore X-100 instrument (GE healthcare, Chalfont St Giles, UK) at 25 °C with buffer HBS-EP+ (10 mm HEPES, pH 7.4, 150 mM NaCl, 3 mM EDTA and 0.05% surfactant P-20). The monoclonal mouse anti-His antibody (SAB2702220, Sigma, US) was immobilized onto a CM5 chip with standard amine coupling. Purified RBD-His was diluted in HBS-EP+ buffer and injected at a concentration of 1 µg/mL for 30 sec at the flow rate of 30 µL/min, followed by injection of 5 different concentration of each mAb with a flow rate of 30 µL/min. The second lowest concentration was repeated to ensure reproducibility, and allowed to dissociate before regeneration with 10 mM Glycine pH 1.7 for 1 min at the flow rate

of 10 µL/min. Referenced and blanked sensorgrams were fitted with BIAcore Evaluation software using a 1:1 Langmuir model of binding. Each assay was performed in duplicate.

Mass spectrometry

A total of 20 µg purified protein was reduced, S-alkylated and digested with trypsin (Promega, USA). Glycopeptides were then analysed by capillary reversed-phase chromatography and electron-spray mass spectrometry using an Agilent Series 6560 LC-IMS-QTOFMS instrument as reported previously [29].

MAb stability assays in human saliva

Saliva was donated by two healthy volunteers and processed immediately after collection. Neither donor had a previous natural infection with SARS-CoV-2 but both had received a two-doses vaccination regime and their salivas had been shown to contained low levels of RBD specific IgG but not SIgA antibodies (Ma, personal communication). The saliva was clarified by centrifugation at 3 000 x g for 15 minutes. Supernatants were collected and aliquoted into 100 µL aliquots before being mixed with 10 µg of each IgG and SIgA mAb variant in a volume less than 5 µL. Following the immediate collection of a 15 µL sample (0 minutes time-point), antibody/saliva solutions were incubated at 37°C and sampled at 5, 60, 150, 240 and 1440 minutes. Samples were analyzed using a sandwich ELISA assay as described above, using plates coated with 150 ng/well purified recombinant RBD-His in PBS pH 7.4. The mAbs/saliva solutions were diluted in blocking buffer 1:1000, added to the wells in normalized concentrations and incubated for 1.5 h at 37°C. The corresponding purified mAb in PBS buffer with known concentration was used as control. IgG and SIgA mAbs were detected using HRP-labelled mouse anti-IgG Fc (AP113P, Merck, Germany) and mouse anti-secretory component (IgA) antibody (SAB4200787, Sigma, US), followed by HRP-labelled anti-mouse antibody (SAB5300168, Sigma, US), respectively.

Virus neutralization assay

Vero E6 cells stably expressing ACE-2 and TMPRSS-2 were obtained by NIBSC, UK and grown in Dulbecco-MEM supplemented with 10% heat inactivated foetal calf serum (FCS, Gibco, Thermo Fisher Scientific, US), penicillin (100 U/ml, Sigma), streptomycin (100 µg/ml, Sigma), Hygromycin B (250 µg/ml, Thermo Fisher Scientific, US) and G418 (250 µg/ml, Thermo Fisher). For plaque reduction assays, cells were seeded to obtain confluent monolayers (10^5 cells/well in 12-well plates) and allowed to settle overnight. Monolayers were visually inspected before use.

SARS-CoV-2 (England/2/2020) was obtained from Public Health England, UK and passaged in Vero E6 stably expressing ACE-2 and TMPRSS-2. Virus stocks were quantified with a standard plaque assay and expressed as plaque forming units per ml (pfu/ml).

Purified mAbs were serially diluted ten-fold starting at 15-20 µg/ml in Dulbecco-MEM with 2% FCS and incubated for 1 h at 37 °C with 30-40 plaque forming units (pfu) of SARS-CoV-2 (England/2/2020). After incubation, the virus-antibody mixture was transferred onto a confluent monolayer of Vero-E6 cells expressing ACE-2 and TMPRSS-2 (NIBSC, UK). After 60 min adsorption at 37 °C, the inoculum was removed and replaced with an overlay containing growth medium (D-MEM with 10% FCS) and 0.8% Avicel (Sigma). The monolayers were incubated at 37 °C, 5% CO2 for 48 h and then fixed and stained with paraformaldehyde 10% (Sigma) and crystal violet (1x, Sigma), respectively. Plaques were counted and expressed as % of a neutralising positive control (WHO International Standard for anti-SARS-CoV-2 immunoglobulin, 20/136, NIBSC, UK). Percentage neutralisation (inhibition) was calculated in MS Excel and GraphPad Prism 9.0.

Protective efficacy of COVA2-15 IgG and SIgA in infected hACE2 transgenic mice

29 8-week-old male hACE2 transgenic mice (C57BL/6J) (T037630, GemPharmatech Co., Ltd., Nanjing, China) were challenged with 1×10^3 PFU SARS-CoV-2 (IVCAS 6.7512). The

mice were split into seven groups (n=3-6) for prophylactic evaluation, as described in (**Figure 5A**). Mice without any challenge and treatment served as blank control (blank, n=3). Mice challenged with SARS-CoV-2 but only PBS buffer as treatment were taken as infection control (PBS, n=4). 250 μg human serum IgG (I4506, Merck, Germany, IgG isotype control, n=4) and human colostrum IgA (I2636, Sigma, US, IgA isotype control, n=4) were administered intranasally 24 h prior to infection and served as isotype treated controls. For the prophylactic group, IgG, SIgA1 or SIgA2 at a dose of 250 μg/mouse (average of 10 mg/kg) was administered intranasally 24 h before infection (COVA2-15 IgG, SIgA1 and SIgA2, -24 h, n=4 or 6). Body weight of each mouse was measured daily. The mice were sacrificed 6 days post infection (dpi) or at the humane endpoint. Lungs were collected for viral load determination and tissue sections for histopathology. Haematoxylin and eosin staining (H&E) and immunohistochemical (IHC) staining were performed, respectively.

Viral load measurement by quantitative RT-PCR

Viral load was detected by quantitative real-time PCR (qRT-PCR) as described previously [30]. Briefly, lung homogenates were prepared by homogenizing perfused whole lung using an electric homogenizer. The supernatant was collected, and total RNA was extracted. Each RNA sample was reverse transcribed to cDNA with RT-PCR Prime Script Kit (Takara, Japan). The cDNA was used in a qRT-PCR reaction with the TaqMan Universal PCR Master Mix (Life Technologies, US), a TaqMan probe (5′-FAM− CAGGTGGAACCTCATCAGGAGATGC −MGB-3′), and primers designed to target the orf1ab gene of SARS-CoV-2 (5′-GTGARATGGTCATGTGTGGCGG -3′ and 5′- CARATGTTAAASACACTATTAGCATA -3′). The samples were run in triplicate on an ABI 7900 Real-Time System (Applied Biosystems, Thermo Fisher Scientific). The following cycling conditions were used: 1 cycle of 50 °C for 2 min, 1 cycle of 95 °C for 10 min, and 40 cycles of 95 °C for 15 sec and 58 °C for 1 min. The virus titer was determined by comparison with a standard curve generated using

RNA extracted from a serially diluted reference viral stock. All experiments were performed in a Biosafety Level 3 facility.

Immunohistochemical *staining of SARS-CoV-2-infected cells in tissues*

Lung tissues were immersed in 10% neutral buffered formalin (Z2902, Sigma, US) for 24 h. After the formalin fixation, the tissues were placed in 70% ethanol and subsequently embedded with paraffin. Tissue sections (4-μm thick) were used for immunohistochemical staining for SARS-CoV-2 detection using the Coronavirus nucleocapsid antibody (40143-MM05, Sino Biological, China). Images were obtained by OLYMPUS IX73 using HCImage Live (×64) software and analyzed by ImageJ (NIH).

Study approval

All animals infected by SARS-CoV-2 were handled in Biosafety Level 3 animal facilities in accordance with the recommendations for care and use of the Institutional Review Board of Wuhan Institute of Virology of the Chinese Academy of Sciences (Ethics Number: WIVA11202003). All the authors declare their compliance with publishing ethics.

Results

Recombinant production of anti-SARS-CoV-2 mucosal antibodies in plants

We generated a panel of four anti-SARS-CoV-2 monomeric IgA and secretory IgA antibodies targeting different epitopes on the spike protein. The variable regions of the well-characterized, neutralizing SARS-CoV-2 specific IgG antibodies COVA2-15[23], COVA1-22 [23], 2-15 [24] and 2E8 were cloned onto IgA1 and IgA2 constant domains for transient expression in glyco-engineered *N. benthamiana* ΔXT/FT plants that are almost completely deficient in β1,2-xylosylation and core α1,3-fucosylation [27]. Light and heavy chain pairs were co-expressed in the presence and absence of the joining chain (JC) and secretory component (SC) to either obtain monomeric or secretory IgA. Immunoblot analysis and ELISA showed highest accumulation of recombinant protein after 5 to 6 days post infiltration. Expression levels of all monomeric IgA1 and IgA2 variants were high and approached those of their IgG counterparts, and all were functional in terms of binding to the SARS-CoV-2 spike protein (**Figure 1A, Figure S1**). However, assembly into multimeric secretory IgA when the JC and SC were co-expressed differed significantly and was highest for COVA2-15, followed by 2E8 and was reduced for COVA1-22 and 2-15 (**Figure 1A**). COVA2-15 and 2E8 variants were therefore selected for further analysis and characterization.

After affinity purification all IgG and IgA isotypes of COVA2-15 and 2E8 were subjected to size-exclusion chromatography. Both COVA2-15 and 2E8 IgG variants display single monodisperse peaks at the expected retention time for proteins with a mass of ~ 150 kDa (**Figure 1B,** dark grey shaded area). COVA2-15 and 2E8 monomeric IgA variants also display a major peak corresponding to the monomeric structural unit with additional minor peaks at lower retention times representing high molecular weight aggregates (**Figure S2**). Co-infiltration of IgA with the JC and SC result in a major peak with minor shoulders at earlier retention times (**Figure 1B**, green/blue shaded area) as well as a second peak representing non-

assembled monomeric IgA (**Figure 1B,** light shaded area). Each of the eluted fraction was analyzed by ELISA to determine the ratio of fully functional and assembled secretory IgA. Recombinant IgAs were captured with RBD and detected with anti-SC antibody and compared to total IgA by using an anti-IgA heavy chain antibody for capture and an anti-kappa or lambda light chain antibody for detection (**Figure 1B,** grey bars). Thereby it was shown that the major peak and its shoulder at higher retention time (green/blue shaded area) of all variants contains fully assembled and functional SIgA, while the peak shoulder observed for COVA2-15 SIgA1 and SIgA2 at an earlier retention time likely contains non-functional high molecular weight aggregates (HMWA). In general, formation of multimeric COVA2-15 and 2E8 IgA variants was very efficient compared to COVA1-22 and 2-15 (**Figure S3**) and previous reports of other multimeric IgA variants in plants [19, 21, 22], whereas COVA2-15 SIgA1 and SIgA2 displayed better assembly than their 2E8 counterparts.

Size-exclusion chromatography fractions containing either the secretory and monomeric IgA species were pooled and were further analyzed using non-reducing SDS-PAGE (**Figure 1C**). Under non-reducing conditions both COVA2-15 and 2E8 mIgA1 and mIgA2 show a predominant band at a molecular mass around 160 kDa representing the fully assembled monomer. Secretory IgA1 and IgA2 variants display a broad band at the expected size of 360 to 400 kDa. Monomeric IgA2 variants displayed additional bands at around 100 kDa and 45 kDa, which likely represent heavy and light chain dimers as the IgA2m(1) isotype used here does not have disulfide bridges linking the heavy and light chains, which are only associated through non-covalent intermolecular interactions [29]. The additional bands observed for monomeric IgA2 were not observed to the same extent for secretory IgA2.

Glycosylation of plant-produced mucosal antibodies

IgA is a heavily glycosylated protein with two predicted *N*-glycosylation sites in the IgA1 heavy chain, four in the IgA2m(1) heavy chain, one in the joining chain and six in the secretory component. In addition, IgA1 has nine potential *O*-glycosylation sites in the proline-rich hinge region, all of which are important post-translational modifications which confer many specific properties of IgA. To assess the glycosylation status of plant-produced IgG, monomeric IgA and secretory IgA isotypes, the purified antibody variants were digested with trypsin and subjected to LC-ESI-MS for analysis of site-specific *N*-glycosylation and the presence of modifications within the IgA1 hinge region (**Figure 1D, Figure S4, Table S1**). The single *N*-glycosylation site in the heavy-chain of COVA2-15 and 2E8 IgG was about 90% occupied and displays a very homogeneous glycosylation profile with the fully processed biantennary complex-type GlcNAc2Man3GlcNAc2 (GnGn) as major glycoform and lesser amounts of GlcNAc1Man3GlcNAc2 (MGn/GnM).

All *N*-glycosylation sites in monomeric and secretory IgA1 and IgA2 heavy chains were fully occupied except the C-terminal *N*-site present in the tailpiece of IgA (NVS) which was only 30 to 70% glycosylated as previously reported for plant-produced IgA [29]. Besides bi-antennary complex type structures (GnGn, MGn) the IgA heavy chains also contained high amounts of oligomannosidic (Man5-9) and paucimannosidic (MM) structures as well as small amounts of complex *N*-glycans carrying the plant-specific core α1,3-fucose resulting from the incomplete silencing of α1,3-fucosyltransferase in the *N. benthamiana* ΔXT/FT line. Furthermore, some site-specific processing can be observed for the NLT site in the CH2 domain of IgA1 and IgA2 which completely lacks α1,3-fucose and displays high amounts of oligomannosidic structures which indicate insufficient secretion or inaccessibility for the respective glycosyltransferases, which is even more pronounced when the secretory component is incorporated.

We were able to detect the single glycopeptide corresponding to the JC of the secretory IgA variants (**Figure 1D, Table S2**). The single *N*-glycan site in the JC of all variants was almost

fully occupied and consisted of oligomannosidic structures, which differs from the very heterogeneously glycosylated JC of mammalian-produced SIgA containing complex-type glycans with high levels of branching and incomplete sialylation [22]. The presence of oligomannosidic *N*-glycans suggests incomplete processing of the JC *N*-glycans in the Golgi of plants.

Furthermore, we were able to identify four individual tryptic glyco-peptides of the secretory component which were all fully occupied and displayed site-specific glycan processing (**Figure 1D, Table S2**). There was little difference between SC glycosylation of SIgA1 and SIgA2, or between COVA2-15 and 2E8 SIgAs. Site NGT exclusively contained oligomannosidic *N*-glycans indicating reduced accessibility for processing at this site. Sites NDT, NYT and NVT mostly consisted of complex-type bi-antennary and paucimannosidic structures (MM > GnGn, MGn), which are likely generated in a post-Golgi compartment by β-hexosaminidases, and completely lacked plant-specific α1,3-fucose [31]. On the hinge region of the plant produced monomeric and secretory IgA1 we detected the conversion of up to six proline residues to hydroxyproline and the addition of variable amounts of arabinoses in 30 to 50% of the converted hinge-regions (**Figure S4, Table S3**).

Stability of anti-SARS-CoV-2 mAbs in human saliva

Due to its unique structural features SIgA is expected to be better suited to survive and function on mucosal surfaces than IgG [32, 33]. To evaluate the stability of plant-produced anti-SARS-CoV-2 IgG and secretory IgA variants in human secretions, an in vitro experiment with COVA2-15 and 2E8 IgG, SIgA1 and SIgA2 was performed using saliva from two donors (**Figure 2**). Each mAb variant was incubated with saliva supernatant, incubated at 37°C and sampled at the times indicated. Time-point samples were analyzed for structural integrity and retained antigen binding capacity by sandwich ELISA capturing using RBD and detection with

383 HRP-conjugated anti IgG-Fc or anti-secretory component. Although the rates of degradation
384 for both IgG and IgA variants based on COVA2-15 and 2E8 varied between experiments when
385 different saliva samples were used, intact IgG was lost at a consistently faster rate over the
386 experimental time-course than secretory IgA variants. The half-life of the SARS-CoV-2 IgG
387 mAbs were calculated using a one phase decay non-linear regression model. Half-lives of
388 COVA2-15 and 2E8 IgG variants were up to 30 minutes and were increased 5 to 10-fold for
389 COVA2-15 SIgAs and 2E8 SIgA2, but were difficult to determine for 2E8 SIgA1 as they did
390 not decline to a plateau in the tested time-frame.
391
392 ***Binding characteristics of different antibody formats to SARS-CoV-2 RBD***
393 Binding of the monomeric and secretory IgA formats to the SARS-CoV-2 receptor binding
394 domain (RBD) was tested using ELISA and the half-maximal effective concentrations (EC_{50})
395 was determined (**Figure 3A, Table S4**). The binding behavior of monomeric and secretory
396 IgA1 and IgA2 was comparable to their IgG counterpart, whereas COVA2-15 variants
397 generally display stronger binding than 2E8 variants. In a competitive ELISA assay COVA2-
398 15 and 2E8 IgG and IgA mAbs were further analyzed for their capability to inhibit RBD
399 binding to the ACE2-receptor (**Figure 3B**). Plant-produced IgG and IgA antibodies were able
400 to inhibit RBD binding to ACE2-Fc using this assay, although 2E8 variants needed to be
401 administered in higher molar ratios. Generally, secretory IgAs performed better, compared with
402 monomeric IgA and IgG as expected due to their multivalency.
403 The binding kinetics of IgG, monomeric and secretory IgA variants of COVA2-15 and 2E8 to
404 RBD were further investigated using surface plasmon resonance (SPR) spectroscopy. RBD
405 was captured with a CM5 chip with immobilized anti-His antibody and different concentrations
406 of each mAb were injected in multi-cycle kinetic experiments and curves were fitted in a 1:1
407 binding model (**Figure 3C**). A rapid association (*ka*) and very low dissociation rate (*kd*) were

characteristic for all COVA2-15 mAb variants, whereas a moderate association and faster dissociation rate was observed for 2E8 IgG. Secretory IgA versions, particularly in the case of 2E8, displayed a more rapid association and a much-reduced dissociation rate with an up to 10-fold increase in affinity (K_D) compared to IgG (**Table 1**). This avidity effect was not observed so clearly for the COVA2-15 variants, likely due to the already near-irreversible nature of the interaction of these monomeric formats with RBD.

Neutralization activity of different antibody formats

The neutralization ability of COVA2-15 and 2E8 IgG and IgA antibodies was investigated using a live virus neutralization assay with a clinical isolate of SARS-COV-2 (England/2/2020) propagated in Vero E6 cells stably expressing ACE2 and TMPRSS-2. Plaques were counted and expressed as % for non-neutralising control (**Figure 4**). All COVA2-15 mAb variants showed high neutralization potential with 50% inhibitory dose (ID_{50}) values ranging from 2 ng/mL to 10 ng/mL, which are in accordance to previously reported data of COVA2-15 IgG variants produced in a mammalian expression system [23].

The RBD-targeting 2E8 mAbs showed reduced capability to block RBD binding to ACE2 in the competition ELISA (**Figure 3B**) suggesting a reduced virus neutralization potency. Indeed, the IgG version of 2E8 exhibited no inhibition at the tested concentrations, monomeric IgA1 and IgA2 were weak neutralizers (ID_{50} ~ 1-2 µg/mL) and only the secretory IgA variants (2E8 SIgA1 ID_{50} ~ 5 ng/mL, (2E8 SIgA2 ID_{50} ~ 20 ng/mL) had strong neutralizing activities (**Figure 4B**).

Efficacy of intranasally administered anti-SARS-CoV-2 mucosal antibodies in ACE2 mice

To compare the prophylactic efficacy of COVA2-15 IgG, SIgA1 and SIgA2 in vivo, mAbs were administrated intranasally to hACE2 transgenic mice 24 hours prior to challenge with

SARS-CoV-2 (**Figure 5A**). High levels of viral RNA (3.4×10^6 copies/mg) were detected in the lungs of control and isotype treated control mice, which were significantly reduced in the prophylactic groups, particularly those treated with 250 μg (average of 10 mg/kg) COVA2-15 IgG, as evidenced by real-time PCR **(Figure 5B**). Significant reduction in viral RNA was also observed in mice treated with 250 μg COVA2-25 SIgA1 or SIgA2. The results correlate with clinical protection, with partial protection afforded by SIgA antibodies and full protection by IgG (**Figure 5C**). Mice receiving COVA2-15 mAbs (IgG and SIgAs) treatment showed less weight loss than the controls (**Figure 5D**). Histopathological analysis of lung tissues demonstrated that SARS-CoV-2 induced lung lesions, focal infiltration of inflammatory cells around bronchi and blood vessels (blue arrows) and alveolar septal thickening (green arrows) in the control mice. There was also narrowing and collapse of the alveolar wall with creation of larger cystic cavities. In the COVA2-15 IgG treated groups, there was little pathology but the appearance of lungs in the SIgA treated groups resembled the PBS treated control group more closely (**Figure 5E**).

Discussion

In this study we investigated the feasibility of producing neutralizing mucosal IgA antibodies against SARS-CoV-2, performed a detailed biochemical and functional analysis of the recombinant antibodies, and explored their potential use to prevent infection in an *in vivo* model. We used the plant-based *Nicotiana benthamiana* ΔXT/FT expression platform for transient production of different monomeric and secretory IgA variants based on several different published IgG antibodies recognizing the SARS-CoV-2 spike protein. All of the monomeric IgG and IgA antibody variants expressed moderately to well and were functional in terms of antigen binding. However, the capacity for assembly into multimeric secretory IgA differed greatly between antibodies with different variable regions. COVA2-15 SIgAs displayed almost full assembly (80-90%) and 2E8 variants demonstrated up to 70% assembly into multimers, thereby exceeding yields and ratios of recombinantly produced SIgA to monomeric IgA in previous reports using plant- and mammalian-based expression [22, 34, 35, 36]. SIgA antibodies based on 2-15 and COVA1-22 on the other hand showed very poor assembly into multimers even though they only differ from COVA2-15 and 2E8 in the variable domain sequences.

In previous studies it was shown that the JC incorporation is the limiting factor for secretory IgA formation [21, 22, 35]. This is consistent with our finding, where we also did not observe an increase of dimeric IgA when the amount of infiltrated JC was varied. Other factors that were reported to contribute to dimer formation were the involvement of certain human chaperones including ERp44 or MZB.1, certain structural features of the CH3 domains of IgA1 and IgA2 and tailpiece glycosylation [21, 22, 37]. Our data indicate that there are also additional factors contributing to Joining chain incorporation and IgA dimerization which need to be investigated further.

Mucosal antibody variants COVA2-15 and 2E8 which displayed highest yield and assembly capacity were selected for detailed characterization. Class-switching of COVA2-15 and 2E8 IgG to monomeric and secretory IgA variants did not significantly influence EC_{50} for binding to the SARS-CoV-2 RBD despite higher valency of SIgAs. However, avidity effects were apparent in SPR kinetic experiments in which the dissociation rate and consequently the dissociation constant (K_D) of 2E8 SIgA compared to the IgG counterpart displaying a moderate affinity, were much enhanced.

Strong binding to RBD and competition with the ACE2 receptor binding translated into potent virus neutralization capacities of all COVA2-15 mAb variants, although no significant increase from monomeric to multimeric antibody formats could be observed despite higher valency of antigen binding sites. This could be due to the already extremely high affinity of monomeric Ig variants. The contrary was observed for 2E8 based antibodies, which showed moderate binding to RBD and reduced competition with ACE2 binding compared with COVA2-15. The monomeric Ig formats of 2E8 displayed little or moderate virus neutralisation, but the multimeric SIgA formats showed strong inhibition. The increased activity of monomeric IgA over IgG might result from the extended hinge region in IgA1 or other structural differences of the antibody classes. Furthermore, IgA and multimeric antibody formats could enhance inhibition of virus entry through other mechanisms such as steric hindrance or increased avidity [38], potentially offering a means of rescuing or re-purposing relatively poorly performing IgG antibodies [36].

Whilst increased valency might confer increased neutralization capacity for some antibody candidates, SIgA is also believed to have a longer half-life in mucosal secretions due to its unique structural features making it less susceptible to proteolysis. SIgA also has unique interactions with structural and functional components of the mucosa and displays non-inflammatory properties [32, 33]. Some of these characteristics are conferred by the extensive *N*-

497 glycosylation of heavy chains and secretory components of IgA [39], which in humans carries
498 mostly branched complex *N*-glycans with high levels of sialic acid and with seven putative
499 sites occupied in varying degrees [40]. This study confirmed that plants are capable of performing
500 these complex post-translational modifications with relatively high homogeneity compared to
501 mammalian production systems and mostly absent *N*-glycan modifications such as β1,2 xylose
502 and α1,3 fucose, which are commonly found in plants that have not been glycoengineered [41,
503 42]. The elongated hinge-region of plant-produced IgA1 on the other hand, exhibits plant-
504 specific conversion of prolines to hydroxyprolines followed by addition of unbranched
505 arabinose chains. Hydroxyproline residues are not found on human proteins such as IgA1 and
506 concerns have been raised that the presence of arabinose chains may bear a risk of an unwanted
507 immune response. Consistent with previous observations of increased half-life for IgA in the
508 mucosa, plant-produced COVA2-15 and 2E8 SIgA variants were significantly more stable in
509 saliva compared to their IgG counterparts [19]. Interestingly, SIgA1 and SIgA2 showed similar
510 rates of degradation, although in humans SIgA1 is more prone to degradation by proteases
511 produced by oral bacteria selectively cleaving sites in the extended hinge-region of IgA1,
512 leaving SIgA2 as the predominant isotype in mucosal secretions [43, 44]. Here, the activity of
513 bacterial proteases on the extended IgA1 hinge-region might be reduced due to the conversion
514 of prolines to hydroxyprolines, which lie within the recognition sequence of many bacterial
515 proteases and are partially extended with arabinose chains, thereby potentially masking the
516 cleavage site [45, 46]. To date there is only limited knowledge about safety and efficacy of the
517 repeated application of recombinant mAbs let alone plant-produced IgAs to mucosal surfaces
518 or influences of plant-specific modifications. However, repeated application of a plant-made
519 SIgA to the oral cavity did not cause any side effects [12].
520 Neutralizing antibodies against SARS-CoV-2 are increasingly used in early treatment of severe
521 COVID-19, but only administered by the systemic rout. SIgAs applied topically to mucosal

sites might provide a different, much earlier intervention to tackle viral carriage and transmission. SARS-CoV-2 is mainly present in the nasopharynx and lungs [47, 48], so direct administration to the upper respiratory tract might provide faster and more robust antiviral activity in the sites, where the virus resides and replicates [48, 49]. Here, the *in vivo* study addressed protection against SARS-CoV-2 challenge in a hACE2 mouse model. This model has the advantage of being strongly informative while being technically straight forward compared to carriage and transmission blocking studies in other animal models. We demonstrated partial protection against SARS-CoV-2 infection in mice treated with plant-produced SIgA1 and SIgA2, but also that the plant-produced IgG COVA2-15 provided complete protection in this model. The apparent superiority of IgG might be due to limitations inherent with the study, specifically the inability to directly compare antibody concentrations for IgG and SIgAs due to different ELISA formats used to quantify concentrations. Additionally, although the murine model is an invaluable system, the upper respiratory murine mucosal microbiota differs to that of humans and can result in an antibody class being favored over another.

In summary, we demonstrated that neutralising monoclonal IgA antibodies against SARS-CoV-2 can be produced as monomeric and secretory formats in a plant-based expression system. We showed that these antibodies are able to maintain their structure and binding affinities when incubated in the harsh environment of human saliva. Importantly, we showed that these plant-generated antibodies have strong virus neutralisation activity and can reduce SARS-CoV-2 infection in an *in vivo* murine model. Therefore, our preliminary data provide strong evidence of the value of secretory IgA in clinical management and/or prevention of COVID-19.

Declaration of interest

The authors declare that the research was conducted in the absence of any commercial or financial relationships that could be construed as a potential conflict of interest.

Author contributions

KG conducted most experiments, analysed the data, and wrote the draft manuscript. SD and RP discovered and cloned 2E8 sequences. EG conducted the in vitro neutralization experiments. RS provided *N. benthamiana* ΔXF/FT plants and glycosylation expertise. CG, RF performed site-specific glycan analysis. FN, HH, YL, YL and QH conducted the animal challenge experiments and evaluated the efficacy of mAbs in SARS-CoV-2 infected transgenic hACE2 mice. JM, KG designed the study, directed and financially supported the study, JM, KG, RS and SD revised the manuscript. All authors critically reviewed the draft manuscript and approved the final version.

Data availability statement

Upon publication the variable domain gene sequences of the 2E8 antibody will be deposited in the Coronavirus Antibody Database, CoV-Ab-Dab (Oxford Protein Informatics Group) and Genbank. Any additional information required to reanalyse the data reported in this paper is available from the lead contact upon request.

Acknowledgements

This work received generous support from the Sir Joseph Hotung Charitable Trust; the European Union's Horizon 2020 programme under Grant Agreements 774078 (Pharma-Factory) and 760331 (Newcotiana); and the Austrian Science Fund Erwin Schrödinger Fellowship J-4583. The MS equipment was kindly provided by the EQ-BOKU VIBT GmbH and the BOKU Core Facility mass spectrometry.

References

1. Speth, M.M. *et al.* Olfactory Dysfunction and Sinonasal Symptomatology in COVID-19: Prevalence, Severity, Timing, and Associated Characteristics. *Otolaryngol Head Neck Surg*, 194599820929185 (2020).

2. Jin, X. *et al.* Epidemiological, clinical and virological characteristics of 74 cases of coronavirus-infected disease 2019 (COVID-19) with gastrointestinal symptoms. *Gut* **69**, 1002-1009 (2020).

3. Peng, L. *et al.* SARS-CoV-2 can be detected in urine, blood, anal swabs, and oropharyngeal swabs specimens. *J Med Virol* **92**, 1676-1680 (2020).

4. Fröberg, J. *et al.* SARS-CoV-2 mucosal antibody development and persistence and their relation to viral load and COVID-19 symptoms. *Nature communications* **12** (2021).

5. Lamm, M.E. & Phillips-Quagliata, J.M. Origin and homing of intestinal IgA antibody-secreting cells. *J Exp Med* **195**, F5-8 (2002).

6. Suleyman, G. *et al.* Clinical Characteristics and Morbidity Associated With Coronavirus Disease 2019 in a Series of Patients in Metropolitan Detroit. *JAMA Netw Open* **3**, e2012270 (2020).

7. Cucchiari, D. *et al.* Cellular and humoral response after MRNA-1273 SARS-CoV-2 vaccine in kidney transplant recipients. *Am J Transplant* **21**, 2727-2739 (2021).

8. Grupper, A. *et al.* Humoral Response to the Pfizer BNT162b2 Vaccine in Patients Undergoing Maintenance Hemodialysis. *Clin J Am Soc Nephrol* **16**, 1037-1042 (2021).

9. Weinreich, D.M. *et al.* REGN-COV2, a Neutralizing Antibody Cocktail, in Outpatients with Covid-19. *New England Journal of Medicine* **384**, 238-251 (2020).

10. Woof, J.M. & Kerr, M.A. The function of immunoglobulin A in immunity. *The Journal of pathology* **208**, 270-282 (2006).

11. Mestecky, J. & McGhee, J.R. Immunoglobulin A (IgA): molecular and cellular interactions involved in IgA biosynthesis and immune response. *Adv Immunol* **40**, 153-245 (1987).

12. Ma, J.K. *et al.* Characterization of a recombinant plant monoclonal secretory antibody and preventive immunotherapy in humans. *Nat Med* **4**, 601-606 (1998).

13. Berdoz, J., Blanc, C.T., Reinhardt, M., Kraehenbuhl, J.P. & Corthesy, B. In vitro comparison of the antigen-binding and stability properties of the various molecular forms of IgA antibodies assembled and produced in CHO cells. *Proc Natl Acad Sci U S A* **96**, 3029-3034 (1999).

14. Teh, A.Y. *et al.* Investigation of a monoclonal antibody against enterotoxigenic Escherichia coli, expressed as secretory IgA1 and IgA2 in plants. *Gut Microbes* **13**, 1-14 (2021).

15. Ma, J.K. *et al.* Generation and assembly of secretory antibodies in plants. *Science (New York, N.Y.)* **268**, 716-719 (1995).

16. Bhaskara, V. *et al.* Efficient production of recombinant secretory IgA against Clostridium difficile toxins in CHO-K1 cells. *Journal of Biotechnology* **331**, 1-13 (2021).

17. Puligedda, R.D. *et al.* Human IgA Monoclonal Antibodies That Neutralize Poliovirus, Produced by Hybridomas and Recombinant Expression. *Antibodies (Basel)* **9** (2020).

18. Boullier, S. *et al.* Secretory IgA-mediated neutralization of Shigella flexneri prevents intestinal tissue destruction by down-regulating inflammatory circuits. *Journal of immunology (Baltimore, Md. : 1950)* **183**, 5879-5885 (2009).

19. Paul, M. *et al.* Characterization of a plant-produced recombinant human secretory IgA with broad neutralizing activity against HIV. *MAbs* **6**, 1585-1597 (2014).

20. Virdi, V., Juarez, P., Boudolf, V. & Depicker, A. Recombinant IgA production for mucosal passive immunization, advancing beyond the hurdles. *Cellular and molecular life sciences : CMLS* **73**, 535-545 (2016).

21. Westerhof, L.B. *et al.* Transient Expression of Secretory IgA In Planta is Optimal Using a Multi-Gene Vector and may be Further Enhanced by Improving Joining Chain Incorporation. *Front Plant Sci* **6**, 1200 (2015).

22. Göritzer, K. *et al.* Efficient N-Glycosylation of the Heavy Chain Tailpiece Promotes the Formation of Plant-Produced Dimeric IgA. *Front Chem* **8**, 346 (2020).

23. Brouwer, P.J.M. *et al.* Potent neutralizing antibodies from COVID-19 patients define multiple targets of vulnerability. *Science (New York, N.Y.)* **369**, 643-650 (2020).

24. Liu, L. *et al.* Potent neutralizing antibodies against multiple epitopes on SARS-CoV-2 spike. *Nature* **584**, 450-456 (2020).

25. Teh, A.Y.-H.C., L; Hu, Y; Kumru, O; Xiong, J; Bolick, DT; Joshi, SB; Grünwald-Gruber, C; Altmann, F; Klempner, M; Guerrant, RA; Volkin, DB; Wang, Y; Ma, J K-C. Investigation of a monoclonal antibody against enterotoxigenic Escherichia coli, expressed as secretory IgA1 and IgA2 in plants. *Gut Microbes* **ISSN 1949-0976 in press** (2020).

26. Peyret, H. & Lomonossoff, G.P. The pEAQ vector series: the easy and quick way to produce recombinant proteins in plants. *Plant molecular biology* **83**, 51-58 (2013).

27. Strasser, R. *et al.* Generation of glyco-engineered Nicotiana benthamiana for the production of monoclonal antibodies with a homogeneous human-like N-glycan structure. *Plant biotechnology journal* **6**, 392-402 (2008).

28. Teh, A.Y., Maresch, D., Klein, K. & Ma, J.K. Characterization of VRC01, a potent and broadly neutralizing anti-HIV mAb, produced in transiently and stably transformed tobacco. *Plant biotechnology journal* **12**, 300-311 (2014).

29. Goritzer, K., Maresch, D., Altmann, F., Obinger, C. & Strasser, R. Exploring site-specific N-glycosylation of HEK293 and plant-produced human IgA isotypes. *Journal of proteome research* **16**, 2560-2570 (2017).

30. Wu, X. *et al.* A potent bispecific nanobody protects hACE2 mice against SARS-CoV-2 infection via intranasal administration. *Cell reports*, 109869 (2021).

31. Shin, Y.J. *et al.* Reduced paucimannosidic N-glycan formation by suppression of a specific beta-hexosaminidase from Nicotiana benthamiana. *Plant biotechnology journal* (2016).

32. Corthésy, B. Recombinant secretory immunoglobulin A in passive immunotherapy: linking immunology and biotechnology. *Curr Pharm Biotechnol* **4**, 51-67 (2003).

33. Corthesy, B. Multi-faceted functions of secretory IgA at mucosal surfaces. *Frontiers in immunology* **4**, 185 (2013).

34. Westerhof, L.B. *et al.* Monomeric IgA can be produced in planta as efficient as IgG, yet receives different N-glycans. *Plant biotechnology journal* **12**, 1333-1342 (2014).

35. Lombana, T.N. *et al.* Production, characterization, and in vivo half-life extension of polymeric IgA molecules in mice. *mAbs* **11**, 1122-1138 (2019).

36. Sun, L. *et al.* Increased in vitro neutralizing activity of SARS-CoV-2 IgA1 dimers compared to monomers and IgG. *Proceedings of the National Academy of Sciences* **118**, e2107148118 (2021).

37. Xiong, E. *et al.* MZB1 promotes the secretion of J-chain-containing dimeric IgA and is critical for the suppression of gut inflammation. *Proc Natl Acad Sci U S A* **116**, 13480-13489 (2019).

38. Yang, H. & Rao, Z. Structural biology of SARS-CoV-2 and implications for therapeutic development. *Nature Reviews Microbiology* (2021).

39. Brandtzaeg, P. Secretory IgA: Designed for Anti-Microbial Defense. *Frontiers in immunology* **4**, 222 (2013).

40. Huang, J. *et al.* Site-specific glycosylation of secretory immunoglobulin A from human colostrum. *Journal of proteome research* **14**, 1335-1349 (2015).

41. Stelter, S. *et al.* Engineering the interactions between a plant-produced HIV antibody and human Fc receptors. *Plant biotechnology journal* **18**, 402-414 (2020).

42. Cabanes-Macheteau, M. *et al.* N-Glycosylation of a mouse IgG expressed in transgenic tobacco plants. *Glycobiology* **9**, 365-372 (1999).

43. Breedveld, A. & van Egmond, M. IgA and FcalphaRI: Pathological Roles and Therapeutic Opportunities. *Frontiers in immunology* **10**, 553 (2019).

44. van Egmond, M. *et al.* IgA and the IgA Fc receptor. *Trends in Immunology* **22**, 205-211 (2001).

45. Novak, J. *et al.* Heterogeneity of O-glycosylation in the hinge region of human IgA1. *Molecular immunology* **37**, 1047-1056 (2000).

46. Mócsai, R. *et al.* Prolyl Hydroxylase Paralogs in Nicotiana benthamiana Show High Similarity With Regard to Substrate Specificity. *Frontiers in Plant Science* **12** (2021).

47. Gallo, O., Locatello, L.G., Mazzoni, A., Novelli, L. & Annunziato, F. The central role of the nasal microenvironment in the transmission, modulation, and clinical progression of SARS-CoV-2 infection. *Mucosal Immunol* **14**, 305-316 (2021).

48. Higgins, T.S. *et al.* Intranasal Antiviral Drug Delivery and Coronavirus Disease 2019 (COVID-19): A State of the Art Review. *Otolaryngol Head Neck Surg* **163**, 682-694 (2020).

49. Cunningham, S. *et al.* Nebulised ALX-0171 for respiratory syncytial virus lower respiratory tract infection in hospitalised children: a double-blind, randomised, placebo-controlled, phase 2b trial. *Lancet Respir Med* **9**, 21-32 (2021).

Figures

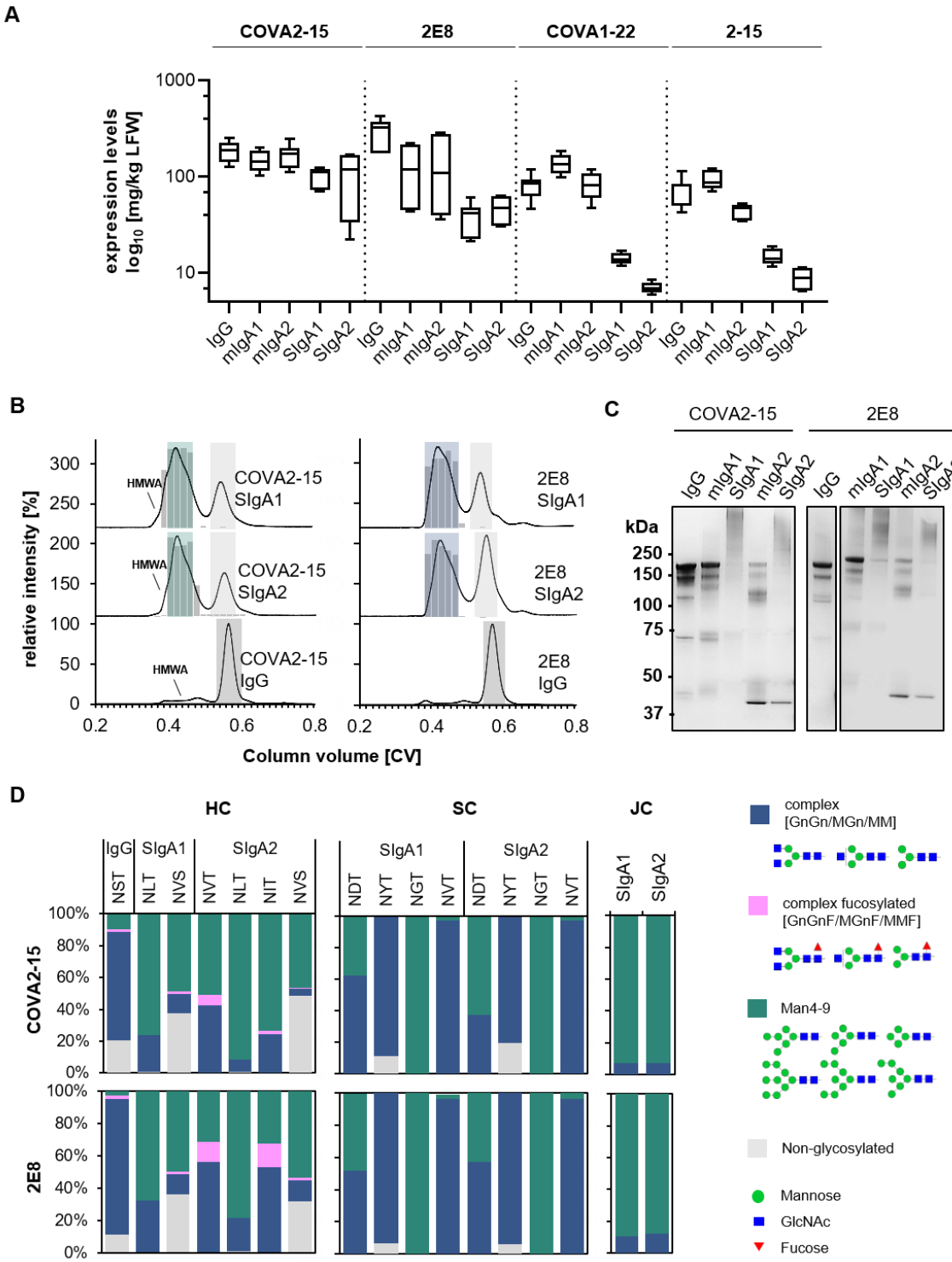

Figure 1: Expression, assembly and purification of monoclonal IgG and different IgA antibodies from *N. benthamiana* plants. (**A**) IgG, monomeric and secretory IgA1 and IgA2 versions of 4 different mAbs recognizing the SARS-CoV-2 spike proteins were transiently expressed in plants. Expression levels were quantified by sandwich ELISA in crude leaf

747 extracts. Detection of monomeric IgA and IgG variants was with either HRP-labeled anti-kappa
748 (COVA2-15) or anti-lambda light chain (2E8, COVA1-22, 2-15) antibodies. SIgA antibodies
749 were detected using anti-secretory component antibodies for all SIgA variants. Quantification
750 data represent the mean of two technical repeats of three independent biological repeats ± SD
751 (**B**) Normalized size-exclusion chromatograms of affinity-purified IgG, secretory IgA1 and
752 secretory IgA2 of the COVA2-15 and 2E8 variants from infiltrated *N. benthamiana* ΔXF
753 leaves. Values were normalized based on the highest signal of each chromatogram. The ratio
754 of secretory IgA to total IgA in each chromatography fraction was determined by ELISA and
755 the relative amount of SIgA in each fraction is indicated by grey bars. Green, blue and grey
756 boxes indicated pooled fractions. (**C**) SDS-PAGE under non-reducing conditions of affinity
757 and size-exclusion purified plant-produced IgG, monomeric and secretory IgA1/IgA2 of
758 COVA2-15 and 2E8 visualized by Coomassie Brilliant Blue staining. (**D**) Site-specific *N*-
759 glycosylation of purified mAbs. Bars represent the relative abundance (%) of glycoforms
760 present at each glycosite of the heavy chains (HC; IgA1: NLT and NVS, IgA2: NVT, NLT,
761 NIT and NVS, IgG1: NST), the secretory component (SC; NDT, NYT, NGT, NVT) and the
762 Joining chain (JC; NIS). N-glycans are abbreviated according to the ProGlycAn system
763 (www.proglycan.com). The symbols for the monosaccharides are drawn according to the
764 nomenclature from the Consortium for Functional Glycomics.
765

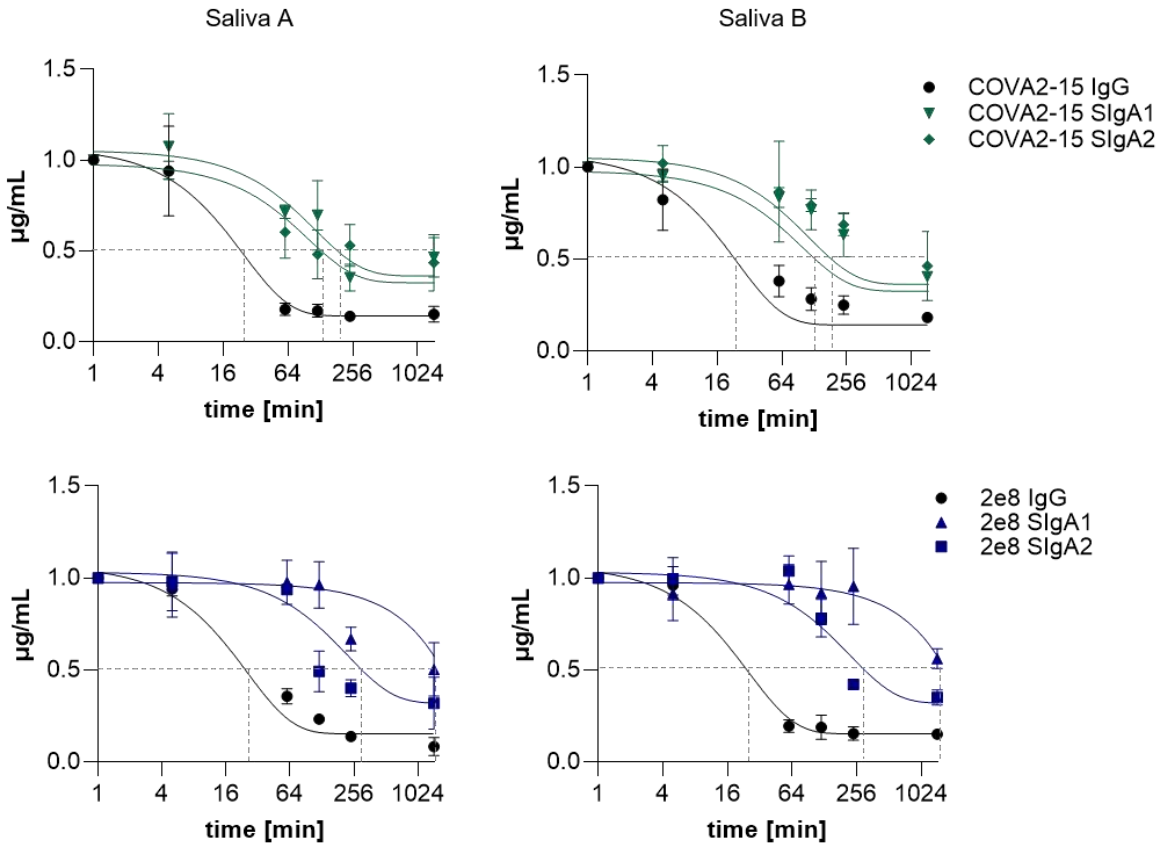

766

767 **Figure 2**: **Stability of COVA2-15 IgG and IgA variants in human saliva**. Saliva from two
768 donors (A and B) was mixed with COVA2-15 and 2E8 IgG and SIgA mAb variants and
769 incubated at 37°C for the indicated time. Samples were analyzed for binding to RBD and
770 assembly through detection with Fc-specific and SC-specific antibodies. The mean ± SD of
771 duplicates is shown. Gray dotted lines indicate half-lives of COVA2-15 and 2E8 variants
772 calculated using a one phase decay non-linear regression model (Graphpad Prism).

773

774

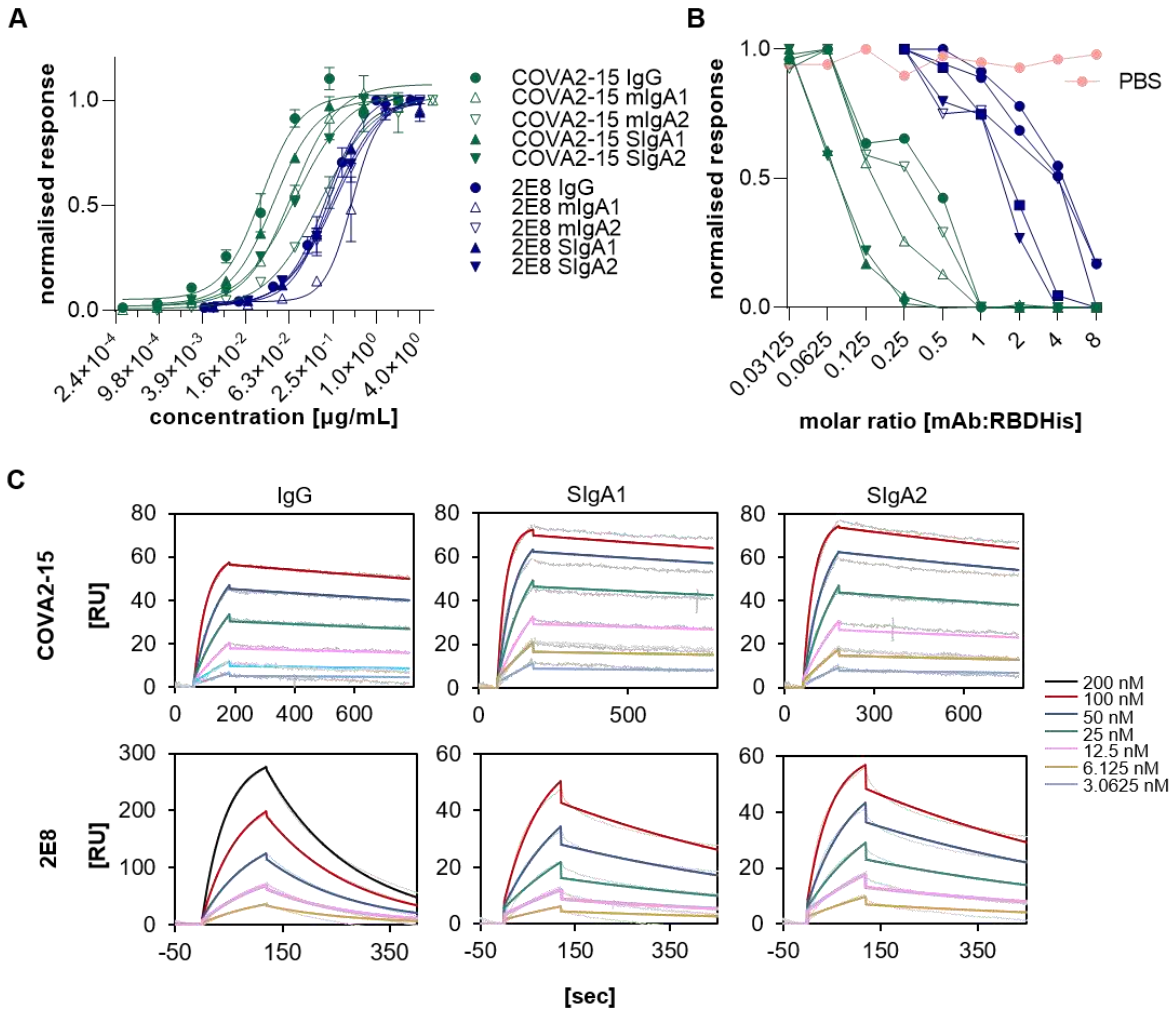

775

776 **Figure 3: Interaction of CoVA2-15 and 2E8 IgG and IgA antibodies with the SARS-CoV-**
777 **2 receptor binding domain (RBD).** (**A**) Determination of EC_{50} values of IgA and IgG anti-
778 SARS-CoV-2 variants to the receptor binding domain (RBD) by ELISA. Each value is the
779 mean ± SD from three independent measurements. (**B**) Inhibition of RBD binding to the ACE2
780 receptor by COVA2-15 and 2E8 mAb variants was determined by a competitive ELISA assay.
781 Data shown is one representative out of two independent experiments with similar results. (**C**)
782 Binding kinetics of COVA2-15 and 2E8 mAb variants to RBD were obtained by SPR
783 spectroscopy in multi-cycle kinetic experiments. An anti-His antibody was immobilized on an
784 CM5 chip, RBDHis was captured (50 RU for COVA2-15 IgG, SIgA1 and SIgA2; 100 RU for
785 2E8 SIgA1, SIgA2; 300 RU for 2E8 IgG), and 5 or 6 different concentrations of the respective

786 mAb were injected. The obtained curves were fitted with a 1:1 binding model. Data shown are
787 from one experiment representative of at least two technical repeats.

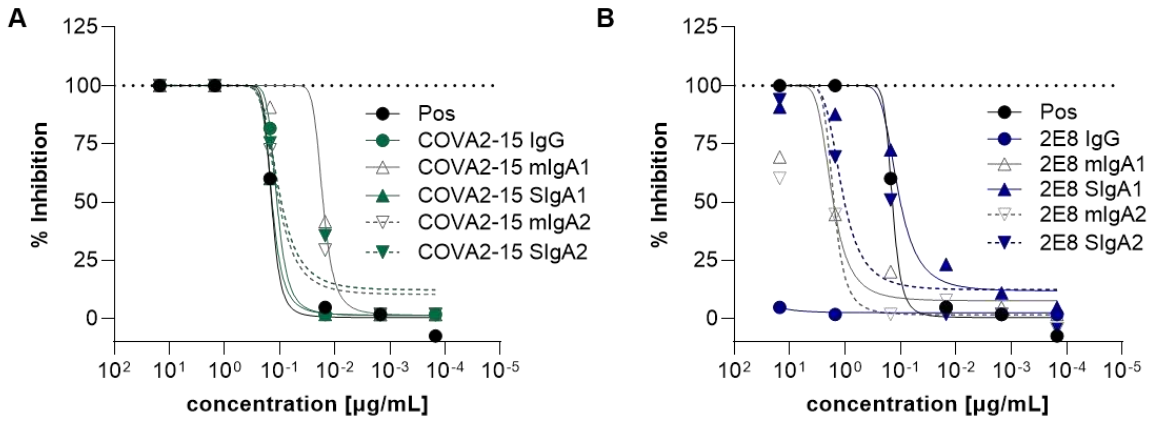

788

789 **Figure 4: Neutralization of SARS-CoV-2 (England 02/2020) by COVA2-15 (A) and 2E8**
790 **(B) mAbs variants.** Neutralization capacity was measured using a PRNT assay on Vero E6
791 cells. MAbs were added in serial 1:10 dilutions starting with 15 µg/mL. A positive control
792 (Pos; WHO International Standard of anti-SARS-CoV-2 immunoglobulin, 20/136, NIBSC,
793 UK) was included. The mean of duplicates of one representative out of two experiments with
794 similar results is shown.

795

A

Group	Name	Reagent	(n)	Antibody infusion -24 h i.n	SARS-CoV-2 challenge 0 h i.n
Group 1	No SARS-COV-2	Blank	3	/	/
Group 2	SARS-COV-2	PBS	4	✓	✓
Group 3	IgA Isotype	Human colostrum IgA	4	✓	✓
Group 4	IgG Isotype	Human serum IgG	4	✓	✓
Group 5	COVA2-15 IgG	COVA2-15 IgG	6	✓	✓
Group 6	COVA2-15 SIgA1	COVA2-15 SIgA1	4	✓	✓
Group 7	COVA2-15 SIgA2	COVA2-15 SIgA2	4	✓	✓

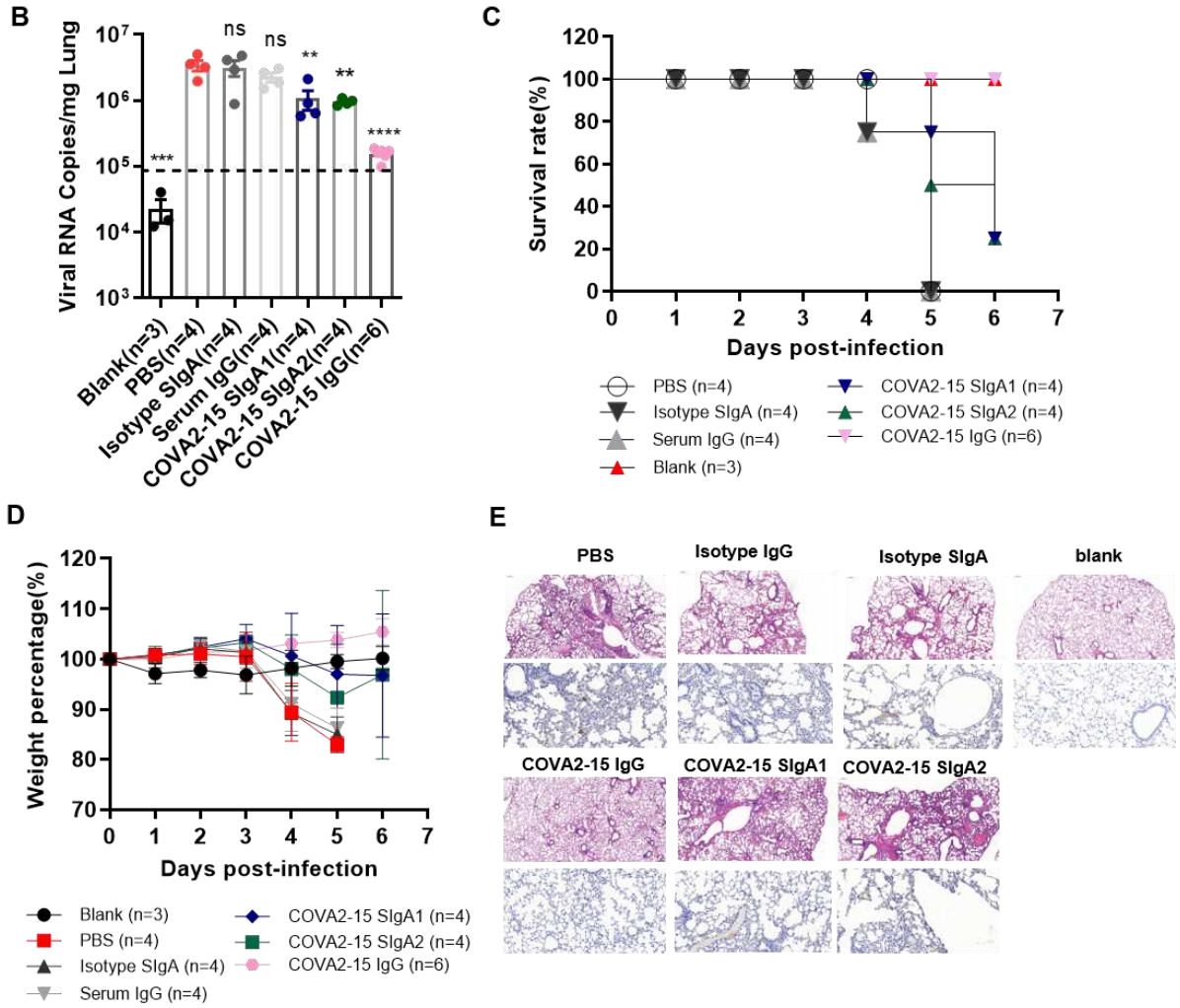

Figure 5: Efficacy of intranasally administered COVA2-15 IgG, SIgA1 and SIgA2 in hACE2 mice. (**A**) Experimental schedule of **COVA2-15** Abs in the prevention and treatment of SARS-CoV-2 infection. The below table summary of groups (n=3-6 mice) with different treatment. (**B**) Viral loads in lung among 7 groups were measured by qRT-PCR. The name of each group in *X* axis was indicated according to table in **A**. Each dot represents one mouse. The limit of detection was $2.3*10^4$ copies/mg referenced to blank control which was not

803 infected with SARS-COV-2 (Blank group). Data represent mean ± SEM. One-way ANOVA
804 was performed to compare treatment group with the PBS control group. ns, no significance;
805 **, P < 0.01, ***, P < 0.001; ****, P < 0.0001. (**C**) Survival rate of all 7 groups were recorded
806 and calculated. (**D**) Body weight of mice among the above 7 groups were recorded. Each line
807 represents data from one group. (**E**) Representative sections of lung were visualized under the
808 × 20 objective. H&E staining was conducted to analyse the lung inflammation and observed at
809 64-fold magnification.

810

Tables

Table 1: Kinetic parameters of COVA2-15 and 2E8 IgG/IgA mAbs to RBD. Rate constants were determined at 5 different concentrations using a 1:1 binding model. Values are shown as mean ± SD of two technical repeats.

	ka (1/Ms)	kd (1/s)	K_D (nM)
COVA2-15 IgG	332930.6 ± 45451.2	0.00024 ± 0.00001	0.74 ± 0.08
COVA2-15 SIgA1	422888.0 ± 66027.9	0.00016 ± 0.00001	0.38 ± 0.02
COVA2-15 SIgA2	326233.2 ± 91502.2	0.00024 ± 0.00003	0.76 ± 0.12
2E8 IgG	70974.3 ± 12795.4	0.00543 ± 0.00080	76.93 ± 2.57
2E8 SIgA1	111255.2 ± 137.2	0.00147 ± 0.00000	13.23 ± 0.02
2E8 SIgA2	155903.3 ± 39703.3	0.00155 ± 0.00003	10.56 ± 2.79

Supplementary Files

This is a list of supplementary files associated with this preprint. Click to download.

- SupplementaryInformation211105.pdf